

Microscopic and Macroscopic Modeling of Non-Isothermal Flow through Porous Media

T. PARIS¹, V. BRUYERE², P. NAMY², D. ROCHAIS³, S. CHUPIN³

¹ CEA Valduc, IS-SUR-TILLE, France

² SIMTEC, 5 rue Felix Poulat, GRENOBLE, France

³ CEA Le Ripault, MONTS, France

Abstract

Macroscopic modeling of fluid flow and thermal diffusion, in a porous medium, requires the description of equivalent properties (permeability, conductivity and diffusivity). However, depending on the microstructure topology of the porous medium and the fluid flow regime at the microscopic scale, great disparities in equivalent properties values can be obtained. The aim of this work is to describe, at the microscopic scale, thermal diffusion and fluid flow for different regimes and quantify how microstructural properties influence macroscopic effective response. After importing the microstructure on a representative volume element (RVE), 2D and 3D strategies are compared. Results are then discussed with literature data and equivalent phenomenological model comparison to validate the numerical approach.

Keywords: Microfluidics – Porous Media – Heat Transfer

Introduction

The three main conservation equations to solve for porous media are dealing with flow and thermal effective properties of the equivalent homogeneous media. A wide range of effective properties can be found in the literature usually bounded by what is referred as volume average and reciprocal average formulations in COMSOL Multiphysics®. These two bounds correspond to specific local organization of porous structures such as parallel and in series pattern.

The real microstructure is a bed of consolidated particles that can't be described exactly without reconstruction from multiple 2D Scanning Electron Microscopy (SEM) or 3D tomography.

In this paper, a numerical strategy is proposed to bridge the gap between the simple effective analytical formulations and the real microstructure approach. These numerical tools reduce the wide range of possible effective properties thanks to some experimental properties of the powder introduced in the numerical twin generation.

This numerical twin generation and the link with COMSOL Multiphysics® calculations are detailed in a first section. Some results and discussions are then emphasized in a second part of this paper.

Numerical Twins & Powder analysis

As briefly mentioned above, two main strategies are available to describe the porous microstructure. The first one is the real microstructure experimental images (SEM or Tomography) that needs reconstruction and numerical transfer to FEM code [1] [2]. This way is sometimes laborious with manual cleaning and filtering to obtain consistent spatial description for FEM calculations and will not be further discussed here.

Another way is based on statistically Representative Volume Element (RVE) calculations with microstructural information (Specific Surface Area (SSA), porosity (ϵ)...) for numerical twin generation. The first step is to generate a given number of spherical particles of a given size in a given box. The size of the box should be given by the invariance of the results to an increasing size and defined as the RVE.

The particle size should be given by the SSA measurement thanks to BET technique for an ideal spherical particle with the relation:

$$S_0 = \frac{6}{d_{eq}} \quad Eq. 1$$

and the maximum porosity should be 0.48 for an ideal and crystallographic organization. The SEM information (figure 1) confirms that the particles aren't so spherical, the distribution is almost bimodal and the porosity is higher than the ideal 0.48 maximum thanks to agglomerates. Moreover volumetric porosity measurement for consolidated media gives approximately 0.7 and laser granulometry analysis concludes to a mean size agglomerates of about 10 [μm].

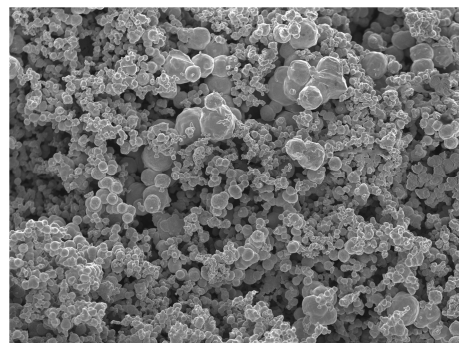


Figure 1 – SEM of powder

All these physical measurements are introduced in the homemade software Genefrac [3] to generate multiple pseudo-RVE and allowing statistically valuable response under the above constraints and computational capacity.

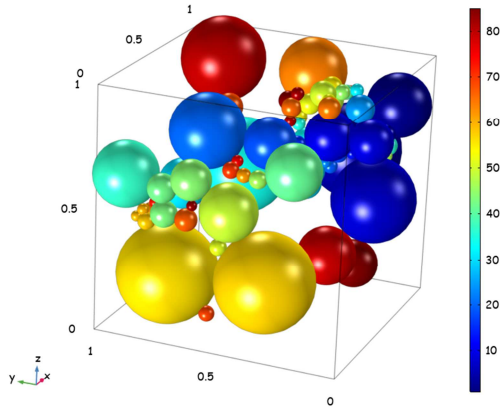


Figure 2 – Pseudo-RVE for bimodal generation

In a first attempt, one simple unimodal microstructure with 26 particles and 400 [nm] diameter with a 50 [nm] overlap allowed that gives 3 agglomerates with particles connections. The obtained porosity is 0.75 with an SSA of 1.17 [m²/g], consistent with experimental measurements.

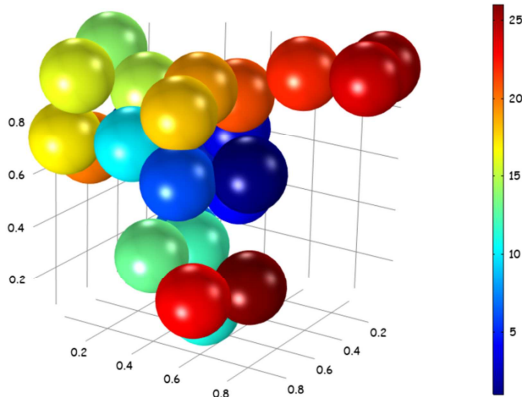


Figure 3 – Pseudo-RVE for unimodal generation

All the 3D coordinates of the particles center are imported in COMSOL Multiphysics® in a txt format (set of points known as point cloud [4]) and a known particle diameter. A scatter volume visualization is now possible (figure 3).

To reduce computational cost, the spatial distribution obtained is projected to a 3D grid of 100x100x10 that give 11 2D slices with refined mapped discretization of 100x100. This is done thanks to a quadratic norm function of coordinates that returns 1 if the coordinate is in a particle and 0 if not. This function is called $cloud(x, y, z)$ and is used as a voxel binary file and could be generated with refined spatial discretization with a refined grid if necessary.

As described in [5], a phase function is defined to identify the location of the solid and void phases in

the microstructure. The following smoothed expression is used for the solid fraction:

$$f_{sol} = flc2hs \left(cloud(x, y, z) - \Delta, \frac{\Delta}{100} \right) \quad Eq. 2$$

with $flc2hs$, a smoothed Heaviside function with a continuous second derivative, $cloud(x, y, z)$ the interpolated function obtained previously, and $\Delta = 0.5$ the threshold value.

A last step is dealing with the link between microstructure and properties evolution (figure 4) where we decided to use a front capturing method (microstructure to material) instead of a front tracking method (microstructure to geometry) for its efficiency (less computational cost) and versatility (coarsening or refining easily).

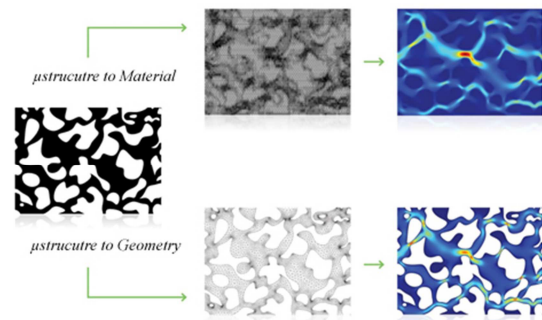


Figure 4 – Microstructure to material and microstructure to geometry strategies, from [6]

This problem has been of a continuous interest over the past years with increasing complexity [7], [8], [9], [10], showing the ability of such a submodeling strategy to evaluate effective properties.

Modeling and Governing Equations

Each “physics” used in COMSOL Multiphysics® is detailed in this section. Both microscale and macroscale equations are presented here. A representation of the 3D microscale geometry (and associated mesh) is given in figure 5 in the corresponding spatial scale. The main objective of this work is to obtain a precise estimation of the thermal diffusion and convective transport in the porous medium as a function of the microstructure.

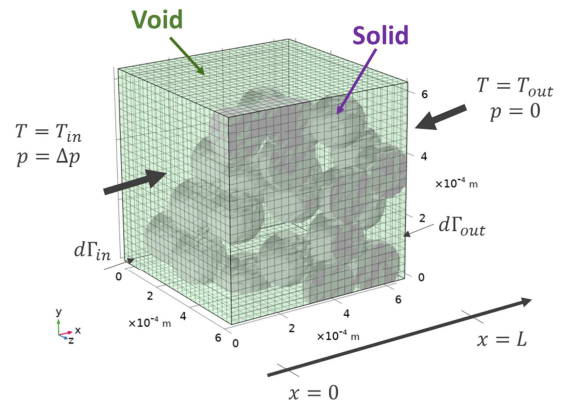


Figure 5 - 3D geometry and mesh representation and boundary conditions

Heat transfer

Due to the treatment of the microstructure with an indicator function $cloud(x, y, z)$, the domains are not geometrically defined and material properties are function of this description. The following heat equation is solved at the microscopic scale.

$$\nabla \cdot (-k_{phase} \nabla T) = 0 \quad Eq. 3$$

where $k_{phase} = k_{sol} f_{sol} + k_{gaz}(1 - f_{sol})$, with k_{sol} is the solid thermal conductivity, k_{gaz} the gas thermal conductivity.

The temperature is set at $T = T_{in}$ at the inlet ($d\Gamma_{in}$, see figure 5) and at $T = T_{out}$ at the outlet ($\partial\Gamma_{out}$). Concerning the other boundaries, thermal insulation is assumed.

An equivalent conductivity is then computed as:

$$k_{eq} = \frac{\iint -k \nabla T d\Gamma_{in}}{(T_{out} - T_{in})L} \quad Eq. 4$$

This value will be compared with values from the literature using a macroscale porous media approach and solving the following equation:

$$\nabla \cdot (-k_{eff} \nabla T) = 0 \quad Eq. 5$$

with k_{eff} is estimated as a function of the porosity of the medium ε , the fluid conductivity k_f and the solid conductivity k_s .

Three options are available in COMSOL Multiphysics® to estimate the effective thermal conductivity which strongly depends on the structure of the porous material:

The volume average method, which represents solid and fluid layers in parallel to the heat flux:

$$k_{eff} = \varepsilon k_f + (1 - \varepsilon) k_s \quad Eq. 6$$

The reciprocal average method, for solid and fluid layer perpendicular to the heat flux:

$$k_{eff} = 1/(\varepsilon/k_f + (1 - \varepsilon)/k_s) \quad Eq. 7$$

The power law method, for a random geometry with similar thermal conductivities for the solid and fluid with:

$$k_{eff} = k_f^\varepsilon \cdot k_s^{(1-\varepsilon)} \quad Eq. 8$$

In the literature, different approaches have been developed to characterize more precisely this coefficient such as the work of Kunii [11], giving the following relation:

$$k_{eff} = k_f \cdot \left(\varepsilon + \frac{(1 - \varepsilon)}{\left(0.22\varepsilon^2 + \frac{2k_f}{3k_s}\right)} \right) \quad Eq. 9$$

The equivalent conductivity k_{eq} , computed from the microscale, will then be compared with effective conductivity, k_{eff} , obtained from the literature.

Fluid Flow

Concerning the fluid flow at the microscopic scale, Navier-Stokes equations are solved in a stationary regime to achieve a precise representation of the permeability of the medium. The following mass and momentum balances equations are solved:

$$\rho \nabla \cdot \mathbf{v} = 0 \quad Eq. 10$$

$$\rho(\mathbf{v} \cdot \nabla) \mathbf{v} = \nabla \cdot [-p\mathbf{l} + \mathbf{K}] + \mathbf{F} \quad Eq. 11$$

with $\mathbf{K} = \mu(\nabla \mathbf{v} + \nabla \mathbf{v}^T)$ the viscous stress tensor function of the viscosity of the fluid, ρ the density, p the pressure field, \mathbf{v} the velocity field and a volume braking force defined by:

$$\mathbf{F} = -K_{num}(x, y, z) * \mathbf{v} \quad Eq. 12$$

As for the heat transfer, the indicator function is used to set the properties of the fluid and the solid. The influence of the K_{num} numerical parameter will be examined in the following section.

Concerning the boundary conditions (see figure 5), a difference of pressure is set, with $p = \Delta p$ at the inlet and $p = 0$ at the outlet. Symmetry conditions are set at the other boundaries.

At macroscopic scale, Darcy's approach is the most commonly used to describe equivalent flow. The mass conservation can be written for the stationary form as:

$$\nabla \cdot (\rho \mathbf{u}) = 0 \quad Eq. 13$$

with \mathbf{u} is the Darcy velocity.

For low Reynolds number and as a first approach the velocity field is often linked to the pressure gradient, with the following linear relation:

$$\mathbf{u} = -\frac{\kappa}{\mu} \nabla p \quad Eq. 14$$

with κ the permeability of the medium.

For non-Darcian flow, the relation between the pressure gradient and the velocity becomes nonlinear and is defined as:

$$\nabla p = -\frac{\mu}{\kappa} \mathbf{u} - \beta \rho |\mathbf{u}| \mathbf{u} \quad \text{with } \beta = \frac{c_F}{\sqrt{\kappa}} \quad Eq. 15$$

The first term is the viscous term corresponding to Darcian flow and the second one is the inertia term proportional to u^2 and β (the inertia factor in [m^{-1}]) can be related to the microstructure morphology with for example the Ergun's relation [12]:

$$\beta = \frac{1.75}{d_{grain}} \frac{(1 - \varepsilon)}{\varepsilon^3} \quad Eq. 16$$

with d_{grain} the characteristic grain size.

To compare macroscopic and microscopic results, an equivalent permeability is defined from the microscopic model as:

$$\kappa_{eq} = \frac{\eta \bar{v} \varepsilon L}{\Delta p} \quad Eq. 17$$

with \bar{v} is the mean velocity, \mathbf{v} , at the inlet boundary. It is important to noticed that the Darcy velocity, \mathbf{u} is related to the velocity of the fluid within the pores (interstitial velocity, \mathbf{v}) by:

$$\mathbf{u} = \varepsilon \cdot \mathbf{v} \quad Eq. 18$$

This equivalent permeability will be compared with classical formulation available in COMSOL Multiphysics® such as Kozeny-Karman relation:

$$\kappa_{Kozeny} = \frac{d_{grain}^2}{180} \frac{\varepsilon^3}{(1 - \varepsilon)^2} \quad Eq. 19$$

Numerical Aspects

Numerical Validation

As a first numerical validation, balances are performed concerning the heat and mass to validate the microscopic model. The relative mass loss is plotted here in figure 6 as a function of the K_{num} coefficient. It is defined by the difference of the inlet mass and the outlet mass divided by the inlet mass. The relative error is very low (below $\approx 10^{-12}\%$), validating the model on a microscopic scale, whatever the K_{num} value.

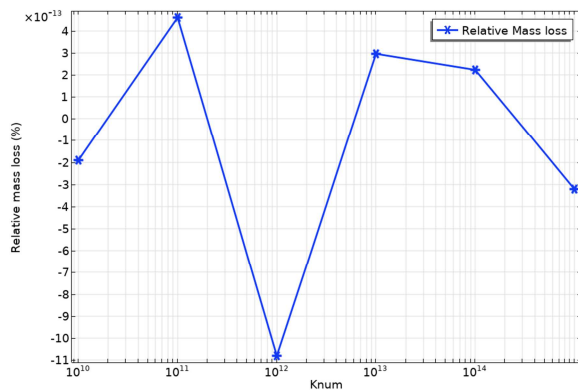


Figure 6 -Relative mass loss (%) as a function of K_{num}

Volume Force Flow

The influence of the K_{num} parameter has also been carefully studied in this work, through its influence on the mass flow. Indeed, to obtain a precise value of the permeability, the model must not be dependent on this numerical penalty parameter. A representation of the evolution of the equivalent permeability as a function of K_{num} is plotted in figure 7. A sufficiently high values of K_{num} ($K_{num} > 10^{14}$) slightly affects the permeability (less than 0.1%) and convergence is obtained.

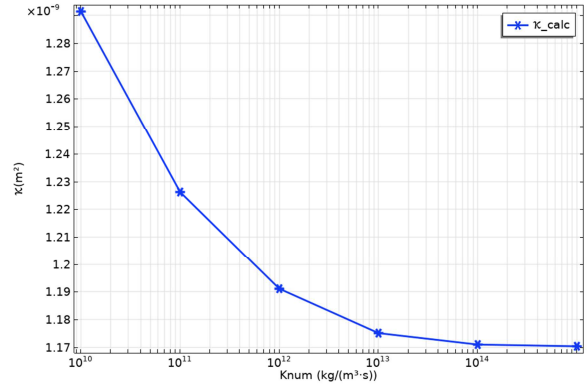


Figure 7. Permeability as a function of K_{num}

Results & Discussion

Thermal / Conductivity

Starting with the 26 particles RVE of figure 3 and boundary conditions imposed as in figure 5 with thermal insulation elsewhere, 11 2D calculations are realized on a 4 cores @2.9[GHz] laptop for approximately 1' of CPU time for each. This saved CPU time gives us the opportunity to realize parametric studies and different microstructure testing.

Only 6 slices of these are presented on figure 8, starting from $z = 0$ to 1 with a step of 0.2 on a normalized box. 11 slices are calculated, and effective conductivities deduced from these calculations are drawn with respect to the mean porosity for each slice (figure 9).

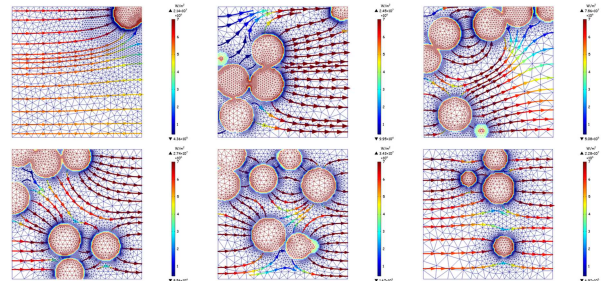


Figure 8 – Local heat fluxes calculated for 2D slices of the 26 particles RVE.

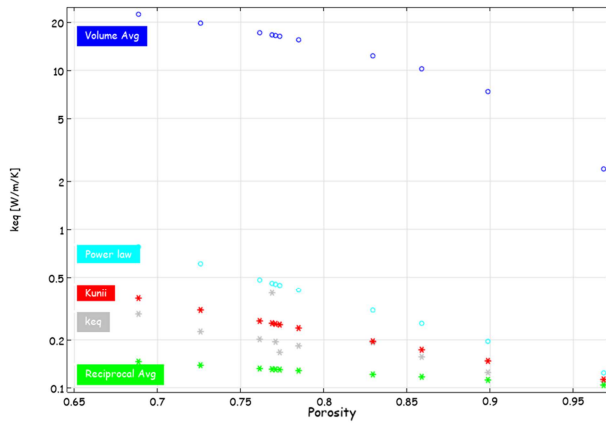


Figure 9 – Effective conductivity vs mean porosity from each 11 slices compared with the 4 analytical models of equations 6 to 9

First of all, global trends are recovered which means that increasing local porosity leads to insulating section (decreasing conductivity).

The effective conductivity (k_{eq} with gray stars on figure 9), obtained by the numerical twin strategy, is close to the Kuniti model and about 2 orders below the default COMSOL Multiphysics® k_{eff} (volume average). The lower bound (reciprocal average) seems to be too low by a factor of 2. k_{eq} is consistent with literature data on this porous medium and gives us confidence about the numerical twin strategy when dealing with thermal effective properties.

Fluid flow / Permeability

Porosity influence

As previously done with effective conductivity, the effective permeability can be evaluated with the boundary conditions imposed as in figure 5 and symmetry otherwise for flow (no penetration and vanishing shear stresses).

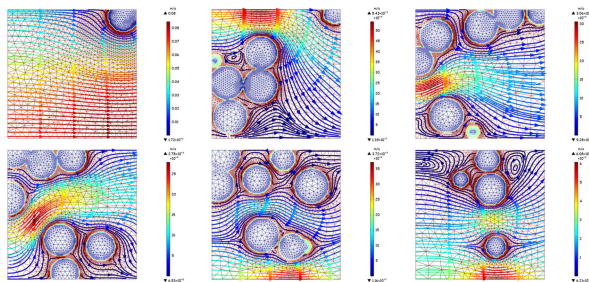


Figure 10 – Local velocity calculated for 6 2D slices of the 26 particles RVE

For this arbitrary imposed pressure gradient, local velocity is low. Creeping and laminar flow give approximately the same responses and this velocity value is consistent with equivalent macroscale calculation for Darcian flow (figure 10). The effective permeability, calculated by the mean of numerical twin strategy, is close to κ_{Kozeny} . The majority of the 2D slices are in between the lower (LB) and upper (UB) bound on figure 11.

A wide variability in permeability (1 decade for 0.05 ϵ_p variation for the 2 2D slices on figure 11) surely dependent on channeling geometry.

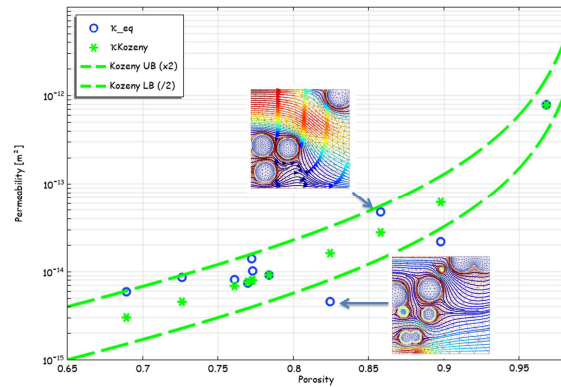


Figure 11 – Effective permeability vs mean porosity from each 11 slices compared Kozeny analytical model

Additional microstructure simulations, not presented in this paper, confirm that homogeneously distributed particles leads to lower permeability evaluation. On the contrary, microstructure with channeling gives higher values.

These results could be interpreted in both ways. The first one is that real channeling could be found in the bed and the second one is that 2D simulations are too flow restrictive. These results suggest that hypothesis for flow simulations should be reconsidered, and 3D simulations have to be further prospected (figure 12).

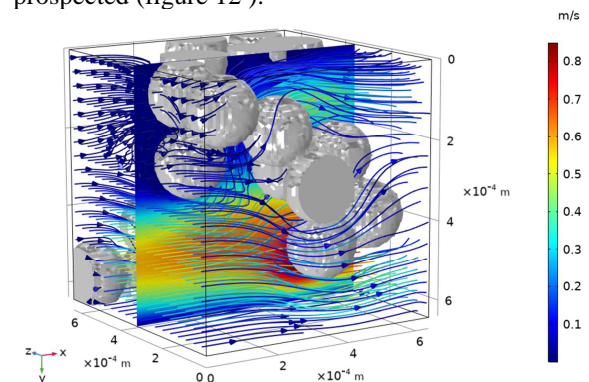


Figure 12 – Example of 3D simulation showing complex 3D flow path

Flow Regimes influence and Reynolds number

A wide scope and interesting topic about flow in porous media address the onset of non-linear behavior, sometimes called the weak inertia regime. The Forchheimer equation (equation 15) is accounted for deviation of the Darcy's law for high Reynolds number and strong inertia regime but the transition regime is usually unclear even if many authors refer to as a critical Reynolds number. This transition zone is given by [11] between $0.1 < Re < 75$, which is quite large, but is in the range of figure 13. After that, the effective permeability calculated starts to drop significantly.

This phenomenon is confirmed with local eddies and wakes that appear with the increasing Reynolds number (figure 14). Some high velocity vectors exist just upstream of lower particle. This is a typical 3D effect. The flow gets around the particle in 3D and 2D simulation could be too restrictive. Strong inertia effects at high Reynolds can be explained by these phenomena.

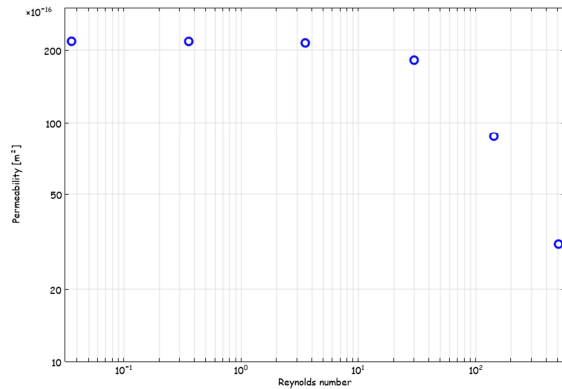


Figure 13 Permeability evolution as a function of the Re

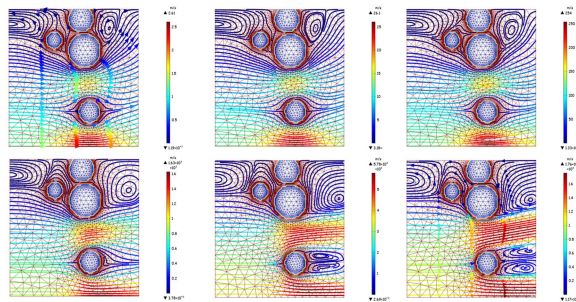


Figure 14 – Local velocity calculated for $z=1$ and increasing Re

Conclusions

A numerical twin strategy linking a homemade software for microstructure generation of consolidated particles with COMSOL Multiphysics® has been proposed. Interesting results enable to bridge the gap between the simple effective analytical formulations and the real microstructure approach. This approach could be considered as a guide line regarding the choice of upscale effective thermal and flow properties for porous media. Different local flow regimes and particles organizations have been shown to strongly influence effective permeability value. As a consequence at macroscopic scale, a special attention should be given to channeling morphology in the bed and local turbulent effects on global response.

Further studies should be investigated to give more confidence about 2D approximations and statically representative results with different microstructure generated.

References

- [1] N. Diaz, A. Jakob, L. Van Loon and D. Grolmund, "Modeling Contaminant Diffusion in Highly Complex Rock Structures," in *COMSOL conference*, 2009.
- [2] S. Zhang, N. Saxena, P. Barthelemy and M. Marsh, "Poromechanics Investigation at Pore-scale Using Digital Rock Physics Laboratory," in *COMSOL conference*, 2011.
- [3] D. Rochais and S. Chupin, Design of porous materials with controlled (conduct)-radiative properties, course of the MATTER school, 2022.
- [4] B. Sjodin, "How to Convert Point Cloud Data to Surfaces and Solids," 2021. [Online].
- [5] B. Sjodin, "How to Generate Randomized Inhomogeneous Material Data," 2017. [Online].
- [6] COMSOL, "Pore Scale Flow," 2017. [Online].
- [7] N. Abdussamie, "Navier-Stokes Solutions for Flow and Transport in Realistic Porous," in *COMSOL conference*, 2010.
- [8] A. Young, "Computing Porosity and Permeability in Porous Media with a Submodel," 2017. [Online].
- [9] N. Bannach, "Modeling Darcian and Non-Darcian Flow in Porous Media," 2020a. [Online].
- [10] N. Bannach, "Thermal Equilibrium and Nonequilibrium Heat Transfer in Porous Media," 2020b. [Online].
- [11] D. Kunii and J. Smith, "Heat transfer characteristics of porous rocks," *A.I.Ch.E. Journal*, vol. 6, p. 71–77, 1960.
- [12] Ö. Akgiray and A. Saatçı, "A New Look at Filter Backwash Hydraulics," *Water Science and Technology: Water Suppl*, vol. 1, no. 2, pp. 65-72, 2001.
- [13] A. Scheidegger, *The Physics of Flow Through Porous Media*, 3rd ed., Univ. of Toronto Press, 1974.
- [14] E. Fontes, "Modeling Approaches in Heterogeneous Catalysis," 2015. [Online].
- [15] B. Meyer and W. Darrel, "Flow through Porous Media: Comparison of Consolidated and Unconsolidated Materials," vol. 24, no. 360-368, 1985.